Transient and Steady-State Shear Banding in a Lamellar Phase as Studied by Rheo-NMR

By Bruno Medronho[1], Ulf Olsson[2], Claudia Schmidt[3], and Petrik Galvosas[4],*

[1] Laboratory of Plant Biotechnology, Faculty of Sciences and Technology, University of Algarve, Campus de Gambelas, Bd. 8, 8005-139 Faro, Portugal
[2] Physical Chemistry, Lund University, PO Box, 124, 22100 Lund, Sweden
[3] Department of Chemistry, Faculty of Science, University of Paderborn, Warburger Straße 100, 33098 Paderborn, Germany
[4] MacDiarmid Institute for Advanced Materials and Nanotechnology, School of Chemical and Physical Sciences, Victoria University of Wellington, PO Box, 600, 6140 Wellington, New Zealand

Dedicated to Professor Hans-Wolfgang Spiess on the occasion of his 70th birthday

Flow fields and shear-induced structures in the lamellar (L_α) phase of the system triethylene glycol mono *n*-decyl ether ($C_{10}E_3$)/water were investigated by NMR velocimetry, diffusometry, and ^{2}H NMR spectroscopy. The transformation from multilamellar vesicles (MLVs) to aligned planar lamellae is accompanied by a transient gradient shear banding. A high-shear-rate band of aligned lamellae forms next to the moving inner wall of the cylindrical Couette shear cell while a low-shear-rate band of the initial MLV structure remains close to the outer stationary wall. The band of layers grows at the expense of the band of MLVs until the transformation is completed. This process scales with the applied strain. Wall slip is a characteristic of the MLV state, while aligned layers show no deviation from Newtonian flow. The homogeneous nature of the opposite transformation from well aligned layers to MLVs *via* an intermediate structure resembling undulated multilamellar cylinders is confirmed. The strain dependence of this transformation appears to be independent of temperature. The shear diagram, which represents the shear-induced structures as a function of temperature and shear rate, contains a transition region between stable layers and stable MLVs. The steady-state structures in the transition region show a continuous change from layer-like at high temperature to MLV-like at lower temperature. These structures are homogeneous on a length scale above a few micrometers.

1. Introduction

Applications of NMR methods in rheological investigations of complex fluids have become more and more popular over the last 20 years [1–5]. NMR spectroscopy can be

---

* Corresponding author. E-mail: petrik.galvosas@vuw.ac.nz

used to probe shear-induced orientations and structures [6,7] while NMR velocimetry yields the flow field in Newtonian and non-Newtonian fluids [8,9]. Further structural information is provided by studying self diffusion and its anisotropy in samples with shear-induced structures [10–16]. These rheo-NMR methods have the advantage that no additional molecules or particles, which may affect the sample properties, are needed as probes and that no requirements concerning the optical properties of the samples exist.

For spectroscopic studies of anisotropic fluids such as thermotropic and lyotropic liquid crystals deuterium NMR is most convenient. The spectra of this $I = 1$ nucleus show a moderate quadrupole splitting and, therefore, are easy to measure and analyze, yielding information about molecular orientation and dynamics [17]. Both spectroscopy on bulk samples and spatially resolved spectroscopy have been used in the field of rheo-NMR. Spatial resolution (NMR imaging) may be achieved by means of slice selection, phase or frequency encoding, or a combination of these methods [9]. The NMR measurement of diffusion and flow is based on the magnetic-field dependence of the resonance frequency and, similar to spectroscopic imaging, requires magnetic field gradients. Most commonly, the technique of pulsed field-gradient NMR is used, which enables signal detection in a homogeneous magnetic field, yielding full spectral resolution [9]. In the pulsed-gradient spin-echo (PGSE) [18] and pulsed-gradient stimulated-echo (PGSTE) [19] experiments a pair of pulsed field gradients leads to a random phase shift and thus a reduced echo intensity (in the case of diffusion) and a coherent phase shift (in the case of flow).

Complex fluids, such as polymers, surfactant solutions, and liquid crystals, are of interest both from a fundamental and a technological point of view [20]. The coupling between structure and flow gives rise to interesting phenomena which may alter the flow properties of a sample considerably and are therefore of relevance in the processing and design of complex fluid materials. Among the lyotropic liquid crystalline phases the lamellar phase is perhaps the most interesting one. Under shear the stacks of amphiphilic bilayers may align with their normal either parallel to the velocity gradient or parallel to the vorticity axis. These orientations have become known as the "c" and "a" orientation, respectively [21]. In addition, a defect structure resembling a dense packing of multilamellar vesicles (MLVs or onions) is found in many cases. Roux and coworkers have shown that the size of these onions is controlled by the applied shear rate [22–25], often decreasing as the inverse square root of the shear rate [23,26]. A large number of studies on shear-induced multilamellar vesicles has followed (*cf.* references in [16], [26], and [27]) but the processes of MLV formation and destruction are still not well understood. Deuterium NMR spectroscopy using D_2O as a probe was found to be a convenient method to investigate both the shear-induced orientations of the lamellar phase and the formation of multilamellar vesicles in situ [26–28]. The D_2O spectra of the "normal" lamellar phase shows a quadrupole splitting, which depends on the orientation of the layers with respect to the magnetic field. When MLVs are formed, the quadrupole doublet collapses to a broad single peak because the water self-diffusion along the curved bilayers of the onion shells and the rotation of the water molecules connected with it occurs just on the right time scale for partial motional narrowing of the spectra. As the MLVs become smaller upon increasing shear rate the line width of the NMR spectra decreases. Therefore, the MLV size can be estimated from the width
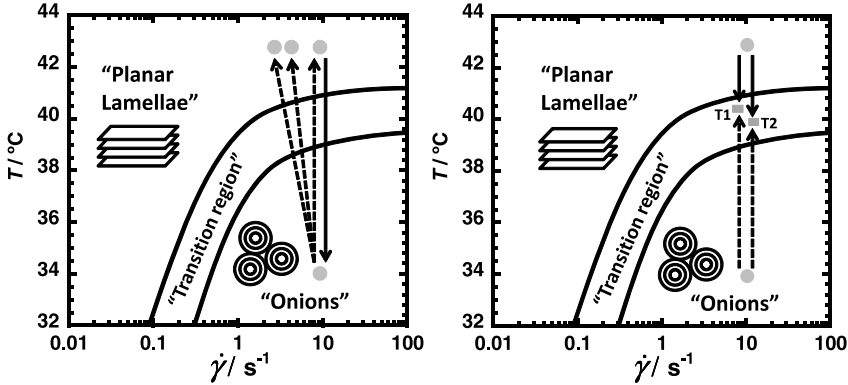
Fig. 1. Shear diagram of the system $C_{10}E_3/D_2O$ (40 % w/w surfactant) [30] showing the stability regions of planar lamellae and MLVs (onions) and the initial and final states of the "jump" experiments. On the left, the experiments involving jumps across the transition region are shown, whereas on the right the jumps into the transition region are indicated.

of the spectra [29]. The characteristic length scale of the MLV structure can also be derived from NMR diffusometry [15].

One of the MLV-forming systems most studied to date is the binary solution of the nonionic surfactant triethylene glycol mono n-decyl ether ($C_{10}E_3$) in D_2O containing 40 wt. % surfactant [16,27,29–37,37–43], although shear-induced MLVs can be found in all surfactants of the C_nE_m type studied so far [26,28,33,44–55]. The shear diagram of $C_{10}E_3$/water (40 wt. %), showing the orientation states as a function of temperature and shear rate, is presented in Fig. 1 [30]. This system has shear regimes of well aligned layers and MLVs in an easily accessible range of temperatures and shear rates. All of our more recent NMR studies on MLVs have been carried out on this system [15,16,27,29,43].

^{2}H NMR spectroscopy under shear has revealed that, while the transformation of aligned planar layers into MLVs is continuous and homogeneous, the reverse process of MLV destruction occurs *via* the nucleation and growth of aligned layers [27]. Spatially resolved ^{2}H NMR and diffusometry has shown that the layers nucleate at the inner moving wall of a Couette cell [16]. By measuring the strain dependence of the diffusion anisotropy in the shear-induced states [16] we could follow the pathway of MLV formation and confirm that an intermediate structure resembling undulated multilamellar cylinders aligned in the velocity direction occurs [32,33,56].

Here, we report additional experiments on the $C_{10}E_3$/water system, using NMR velocimetry to study the dynamics of the system in addition to structural investigations using diffusometry and spectroscopy. By means of velocimetry the phenomenon of shear banding [57–60] can be investigated. Gradient shear banding, that is the occurence of bands with different shear rates, stacked along the velocity gradient, is a likely scenario during the inhomogeneous MLV-to-layer transition [16] since MLVs and aligned lamellae have different viscosities. There has also been a report on the observation of vorticity shear banding, *i.e.*, of bands of different stress stacked along the vorticity axis, during the lamellar-to-onion transition [61] but we have seen no evidence

of this in our NMR studies. In addition, we will present NMR experiments carried out to reveal the structure in the "transition region" which separates the two regimes of shear-induced aligned lamellae at high temperature and MLVs at low temperature, shown in Fig. 1.

2. Materials and methods/experimental

2.1 The system $C_{10}E_3/D_2O$

Triethylene glycol mono *n*-decyl ether ($C_{10}E_3$) was purchased from Nikko Chemical Co. (Tokyo, Japan) (purity higher than 99.8 %). Deuterium oxide (D_2O) with a purity of 99.9 % was supplied by Sigma Chemicals (Steinheim, Germany). Samples were prepared by weighing 40 wt % of surfactant and 60 wt % of water into vials. The two components were thoroughly mixed and subsequently centrifuged in order to remove air bubbles. All samples were prepared with a ratio D_2O/H_2O of 9 : 1 by weight.

2.2 NMR apparatus and rheo-NMR devices

All experiments have been conducted on a Bruker Avance spectrometer operating at a ^{1}H resonance frequency of 400 MHz. Gradients of up to 1.45 T/m for NMR diffusometry and velocimetry were provided by a Micro2.5 three-axes micro-imaging system (Bruker). The temperature of the sample was kept constant *via* the conventional Bruker temperature control. However, to avoid temperature gradients over the sample volume, the temperature of the gradient coolant was set to the same temperature as the target sample temperature. Sample temperatures were within ± 0.5 K of the desired temperature which was verified once prior to the experiments *via* a temperature sensor situated in a liquid filled NMR sample tube in place of the Couette cell. The same setup allowed to confirm that temperature equilibration after temperature jumps was completed after 40 min.

The properties of the surfactant solution were studied in the gap of a concentric cylinder rheo-NMR Couette device (see Fig. 2 left) with an inner rotating tube (outer diameter 16 mm) placed inside an outer stationary tube (inner diameter 18 mm) resulting in a fluid gap of 1 mm. Teflon spacers in the gap between cylinders ensure concentricity and smooth rotation of the inner cylinder. The outer, stationary tube is held by the NMR coil assembly while the inner tube is turned by a stepper motor *via* a gear box (with a ratio 50 : 1) and a rigid mechanical drive shaft [1]. The stepper motor is able to apply rotations in the frequency range 0.1 Hz to 14 Hz which generates shear rates of interest for the different experiments. Gap-average shear rates were calculated as

$$\dot{\gamma} = \frac{r_i \omega_i}{r_o - r_i} \, , \tag{1}$$

valid for small gap sizes [62]. The radii of the outer and inner cylinders are r_o and r_i, respectively, while ω_i is the inner cylinder angular velocity. Actual shear rates deviate by about ± 10 % from the gap-average.
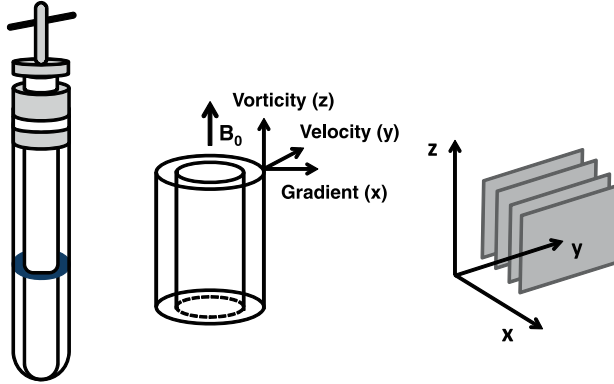
Fig. 2. Schematic illustration of the Couette geometry used (left). The schematic in the middle relates the shear frame with its velocity gradient, velocity and vorticity directions to x, y and z of the laboratory coordinate system defined by the static magnetic field (z) and the magnetic field gradients (x, y, and z). On the right the orientation of aligned planar lamellae (in the "c" direction) in the shear frame is shown.

2.3 Rheo-NMR experiments

2.3.1 Velocimetry

1D NMR imaging was used in combination with the PGSTE for the acquisition of the velocity field across the Couette cell gap in the sheared sample [63]. The NMR pulse sequence used is shown in Fig. 3. The two gradients in the PGSTE part are incremented in steps simultaneously. This creates a residual phase shift after the second gradient pulse which is a measure of the velocity v_y in the direction of the magnetic field gradient expressed by the collective displacement $\Delta y = v_y \Delta$ of the molecules during the observation time Δ:

$$\Delta\phi = \gamma g_y \delta \Delta y. \tag{2}$$

Here, g_y and δ are the gradient strength and width, respectively. γ is the gyromagnetic ratio. Actual velocities may be extracted from the measurement either by direct evaluation of Eq. (2) using recorded residual phase shifts $\Delta\phi$ or by using the concept of dynamic NMR microscopy [64]. This concept utilises Fourier transforms with respect to the imaging gradients as well as the PGSE gradients. The latter delivers the averaged propagator and the mean velocity with it while the former provides spatial resolution and is accomplished by the imaging part of the pulse sequence using a double slice selection scheme. The first slice is positioned across the centre of the cell, oriented along the x, z-plane with a width of 2 mm. This selects two opposite strips from the annular gap, ensuring that influences from the curvature of the Couette cell can be neglected, allowing one to operate in a Cartesian coordinate system of velocity gradient (x), velocity (y) and vorticity (z) as indicated in Fig. 2. The second slice is oriented perpendicular to the first one along the x, y-plane with a width of 40 mm, excluding undesired parts of the sample such as the semi-spherical end of the Couette cell. 1D imaging is performed
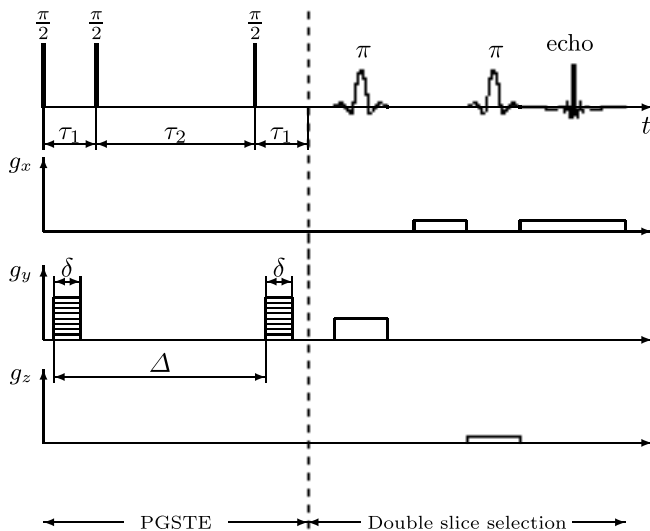
Fig. 3. Radiofrequency and magnetic field gradient pulse sequences for the acquisition of velocity fields. Two magnetic field gradient pulses of duration δ and separation Δ are applied in the y-direction and increased successively in amplitude. Two soft 180° pulses are used in combination with magnetic field slice gradients in the y and z-direction to select a specific volume of spins.

via frequency encoding in x direction along the velocity gradient, ultimately recording and mapping the velocity field across the gap of the cell in the two strips.

Velocity images (maps) were recorded during transitions from the MLV to planar lamellae at shear rates of $10\,\mathrm{s}^{-1}$, $5\,\mathrm{s}^{-1}$ and $2.5\,\mathrm{s}^{-1}$. The opposite transition from lamellae to MLVs was studied at $10\,\mathrm{s}^{-1}$. Likewise, for a shear rate of $10\,\mathrm{s}^{-1}$ velocity fields were acquired after jumping into the transition region. Corresponding maps were obtained with a spatial resolution of $100\,\mu\mathrm{m}/\mathrm{pix}$ resulting in a resolution of 10 pixels across the gap. The observation time was set to $\Delta = 20\,\mathrm{ms}$ and the gradient width to $\delta = 1\,\mathrm{ms}$. 4 PGSE gradient values were used up to a maximum gradient of $g_y^{\mathrm{max}} = 0.44\,\mathrm{T/m}$ (for the smallest shear rate). A total of 4 scans were acquired for each PGSE gradient step with a repetition time of 6 s, resulting in a total time of 96 s per velocity image. To follow the velocity field in the gap over time images were recorded continuously (up to 80) while the sample was under constant shear.

2.3.2 Diffusometry

The spatially resolved measurement of diffusivities (diffusion imaging) is very similar to the concept of velocity imaging. In fact it uses the same pulse sequence (with the only alteration that the PGSTE gradient pair in Fig. 3 may also be applied in x or z direction for measuring the corresponding diffusivities). The main difference is that measurements are carried out while the sample is at rest. This results in a start-stop experimental protocol with periods of shearing (increasing the strain) interspersed by periods of zero shear while acquiring data. It was verified by previous studies that the structure is quenched into a metastable state for at least 30 min [16], which allows for

the time required by the diffusion experiments. This holds even for rapid transitions which are completed typically after several thousand strain units, corresponding to only several hundred seconds at a shear rate of $10 \, \mathrm{s}^{-1}$.

It is also evident that no residual coherent phase shift as expressed by Eq. (2) will occur. Instead diffusive motion will cause a random phase spread which relates to the diffusion coefficient D *via* the Stejskal–Tanner equation [18]

$$E = E_0 \exp \left\{ -D \left(\gamma \delta g \right)^2 \left(\Delta - \frac{1}{3} \delta \right) \right\} = E_0 \, \mathrm{e}^{-Db} . \tag{3}$$

E_0 is the signal amplitude without pulsed magnetic field gradients applied. It is convenient to introduce the so called *b*-factor, as given by Eq. (3), which represents all parameters controlled by the experiment. The diffusion images were recorded with similar parameters as compared to the velocity images. However, the gradient width and amplitude of the PGSTE pair was increased to $\delta = 5$ ms and $g^{\mathrm{max}} = 1.33$ T/m (16 gradient steps) which accounts for the smaller displacements caused by diffusion only. The number of scans is increased from 4 to 8.

As for the velocity images the obtained data sets are two-dimensional. The image dimension is processed *via* Fourier transform leading to 1D images with 10 pixels across the Couette cell gap (identical to the velocity images). The second dimension (along the increasing PGSTE gradients), however, does not obey Eq. (2) anymore. Instead this dimension was now processed by fitting Eq. (3) to the obtained data leading to the diffusion coefficients for each individual pixel. The interested reader may find further details on the experimental conditions and the data processing in [16]. Some of the acquired data did not fit satisfactorily to a mono-exponential decay as expressed by Eq. (3). While this may indicate slight structural inhomogeneities across the sample it was outside the scope of this study to investigate this behavior further. Therefore, the averaged diffusion coefficient as obtained from the initial signal decay was used in these cases.

2.4 ^{2}H NMR

The quadrupolar splitting of the deuterium nucleus was used to assess the amount of order in the sample as characteristic for the different structures. Since planar lamellae are globally oriented in the gap with their director being perpendicular to z one expects to see a doublet in the ^{2}H NMR spectra of heavy water. This doublet results from the residual quadrupole coupling due to the anisotropic environment of the heavy water molecules. Its splitting reflects both the orientation of the phase axis (here the orientation of the layer normal, being perpendicular to the magnetic field) and the local orientational order parameter of heavy water (which is about one tenth of the order parameter of the surfactant). The situation for MLVs is different since the lamellar layers are strongly curved. Therefore all orientations of the surface director will be present in the sample and diffusion of the water molecules along the surface results in partial motional narrowing, leading to only a single peak in the deuterium spectra as a characteristic signature for MLVs [28].

Deuterium spectra have been acquired with a spectral width of 5 kHz allowing to record the wide spectra originating from the MLVs. Spectra were acquired continuously

while the sample was under shear, thus recording the structural change in the sample over time.

3. Results and discussion

3.1 Shear banding during the transition from multilamellar vesicles to planar layers

According to the shear diagram of $C_{10}E_3/D_2O$ (40 wt. % surfactant) shown in Fig. 1, MLVs are not stable at temperatures above about 41 °C. Thus, when a sample consisting of shear-induced MLVs is sheared at higher temperature the MLVs are destroyed and a state of planar lamellae aligned parallel to the velocity-vorticity plane is obtained. This shear-induced transition has previously been found to resemble a nucleation-and-growth process, in which the layers start to grow from the inner moving wall of the Couette cell [16]. Using spatially resolved NMR diffusometry and velocimetry the MLV-to-layer transition is investigated here in more detail. The protocol for these experiments is represented by the arrows shown in Fig. 1, left. As indicated by the arrows pointing upwards, MLVs were initially prepared by shearing at $\dot{\gamma} = 10\,\text{s}^{-1}$ and 34 °C for 60 min. Then shear was stopped, the temperature was changed to 43 °C, where MLVs are not stable under shear, and after 45 min to allow for temperature equilibration, shear was started again at the desired shear rate. While the sample continued to be sheared when measuring velocities, shear was interrupted for diffusion measurements, employing the start-stop protocol described in Sect. 2.3.2 above.

Figures 4 to 7 show the results obtained when the formation of layers takes place at $\dot{\gamma} = 10\,\text{s}^{-1}$ (vertical upward arrow in Fig. 1, left). As reported previously [16], spatial inhomogeneities during the transformation process lead to diffusivities that vary as a function of the radial position across the annular gap of the shear cell. This can be also seen in Fig. 4, in which profiles of the diffusivity in the velocity direction are presented for selected strain values. In this and all the following viewgraphs depicting spatial profiles, the wall of the inner moving cylinder is to the left at 0 mm and the outer stationary wall is positioned at 1 mm. The diffusion profiles reveal that the formation of layers, having a higher diffusivity along y than MLVs, does not occur simultaneously everywhere in the gap. Already at the lowest strain of 200, a region with the higher diffusion coefficient corresponding to layers is observed close to the inner wall. As γ increases, the interface between the regions of layers and MLVs moves towards the outer stationary wall of the Couette cell, until the transition is completed and D is the same everywhere in the gap. This is in good agreement with our previous diffusion results obtained with another shear cell, possessing a somewhat wider gap of 1.5 mm, and by ^{2}H NMR imaging [16]. At $\gamma = 1800$ a second narrow region of fast diffusion can be observed at the outer wall, *cf.* Fig. 4. Similar observations, typically at higher strains, were made in additional diffusion experiments not presented here, but not by velocimetry. We will return to this issue later.

Since aligned layers have a lower viscosity than MLVs [25,26] one can expect the shear rate to be higher in the part of the sample consisting of layers. By means of velocity imaging we have investigated whether the observed regions with different structures do indeed correspond to bands of different shear rate. In a separate experi-
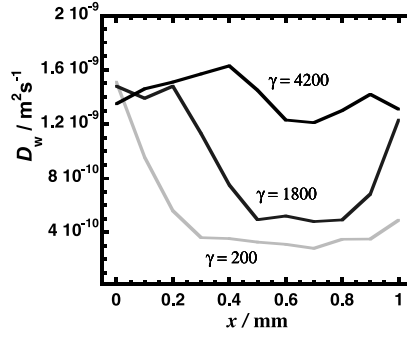
Fig. 4. Diffusion coefficient along the velocity direction as a function of the position in the gap for different strain values during the transition from MLVs to planar lamellae at 43 °C and $\dot{\gamma} = 10\,\text{s}^{-1}$.
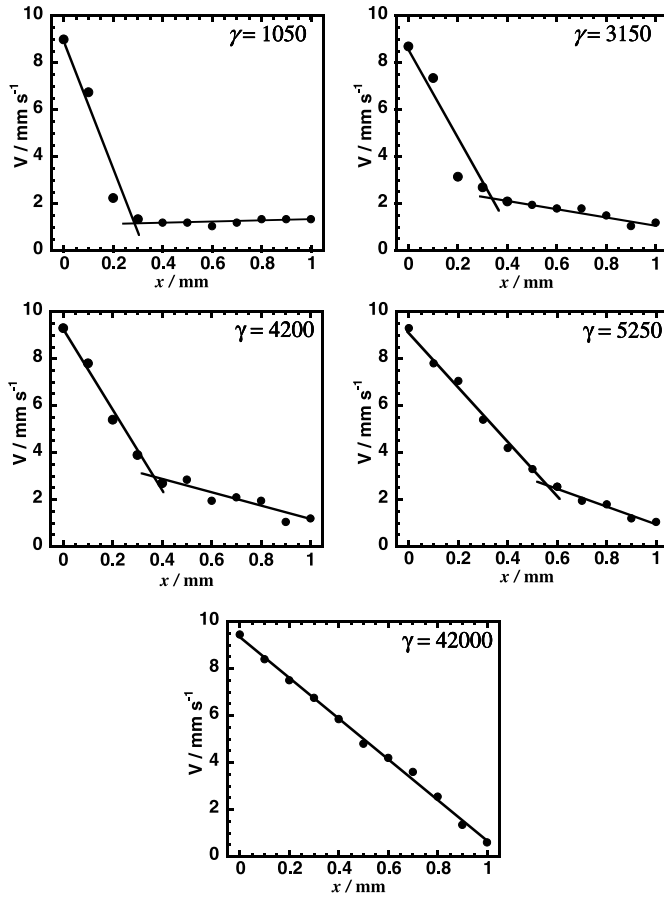

Fig. 5. Velocity profiles across the gap for different strain values during the transition from MLVs to planar lamellae at 43 °C and $\dot{\gamma} = 10\,\text{s}^{-1}$. Bands of low and high shear rate can be distinguished. The average shear rates are obtained by linear fits.
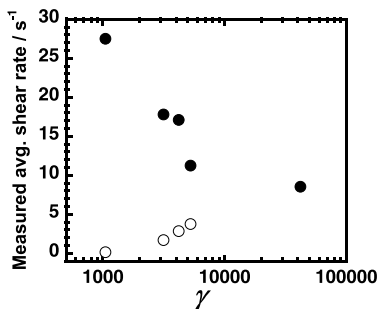
Fig. 6. Average shear rates in the two bands during the transition from MLVs to planar lamellae at 43 °C and $\dot{\gamma} = 10\,\mathrm{s}^{-1}$.
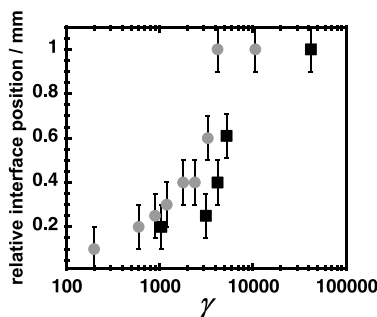

Fig. 7. Position of the interface between planar lamellae and MLVs obtained by diffusometry (gray circles) and between the bands of high shear rate and low shear rate determined by velocimetry (black squares) during the transition from MLVs to planar lamellae at 43 °C and $\dot{\gamma} = 10\,\mathrm{s}^{-1}$.

ment, starting again from MLVs generated at 34 °C by shearing at $\dot{\gamma} = 10\,\mathrm{s}^{-1}$, the profiles of the velocity component in the direction of flow were measured. The results are shown in Fig. 5. At lower strains, two regions of different slopes, indicating two bands of different shear rates, can be clearly distinguished. The interface between the band of high shear rate moves from the inner wall towards the outer wall until, at large strain, there is only one region of uniform shear rate. The average shear rates in each band, obtained by linear regression as shown in Fig. 5, are presented in Fig. 6.

In Fig. 7, the interface between the two shear bands extracted from the velocity profiles in Fig. 5 is compared with the interface between the regions of different diffusion coefficients as obtained by diffusometry (*cf.* Fig. 4). The results from the two different methods agree very well. In our previous work a fairly good agreement between the interface positions observed by diffusometry and ^{2}H NMR imaging was found [16]. We can thus conclude that, within experimental error, the shear rate bands correspond to bands of different structures.

Velocimetry monitoring the MLV-to-layer transition starting from the same initial state as before was also performed at shear rates of 5 and 2.5 s^{-1} (*cf.* additional upward arrows in Fig. 1, left). The results are summarized in Fig. 8. The velocity profiles shown
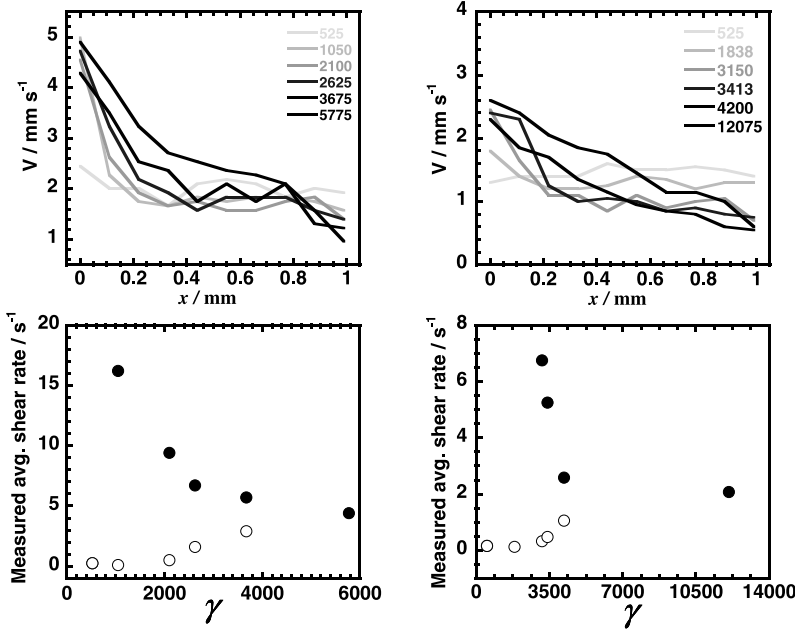
Fig. 8. Velocity profiles (top) and average shear rates (bottom) during the transition from MLVs to planar lamellae at 43 °C and $\dot{\gamma} = 5\,\mathrm{s}^{-1}$ (left) and $2.5\,\mathrm{s}^{-1}$ (right).

on top of Fig. 8 illustrate once more that the band of low shear rate at the outer wall, which is initially present and corresponds to MLVs, shrinks with increasing strain. This shrinkage matches the creation and growth of a high-shear-rate band near the wall of the rotating cylinder, until a single band corresponding to planar layers is obtained. The shear rates extracted by linear fitting of the velocity profiles are presented in the bottom of Fig. 8. The results are in keeping with the observations at the higher shear rate.

The boundaries between the shear bands obtained for all three shear rates investigated by velocimetry are compared in Fig. 9. When the position of the boundary is plotted as a function of strain the data fall on one curve, demonstrating that the MLV-to-layer transition scales with the applied strain and does not depend on the applied shear rate. This is in agreement with previous findings for the same system based on an analysis of ²H NMR line shapes [27]. Strain scaling has also been observed in the case of shear-induced alignment of the lyotropic hexagonal phase [65,66].

3.2 Shear effect on the defect density

In the previous section we have discussed the shear-induced destruction of vesicles and their transformation into planar lamellae. Before turning to the reverse transformation from layers into vesicles, we will stay for a moment within in the stability regime of layers and consider the influence of shear on the structure of the system. Previously, shear flow had been observed to induce structural defects in the lamellar structure even if no subsequent transition to MLVs follows [43] and the shear-rate was determined as
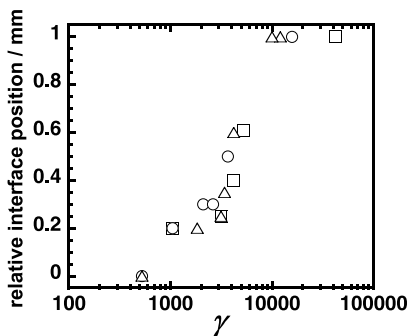
Fig. 9. Position of the interface between the bands of low and high shear rate during the transition from MLVs to planar lamellae at 43 °C for the three different shear rates investigated. Triangles, circles, and squares correspond to shear rates of 2.5, 5, and $10\,\text{s}^{-1}$, respectively.
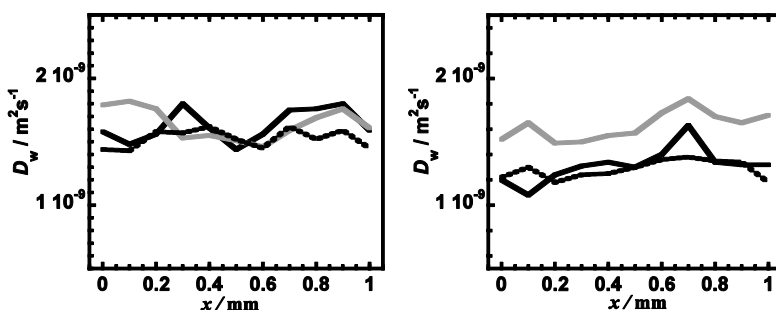

Fig. 10. Profiles of the water diffusion coefficients in the velocity (left) and vorticity (right) direction as a function of the applied shear rate at 43 °C within the region of planar lamellae after shearing at rates of 10, 0.1, and again at $10\,\text{s}^{-1}$. The black, grey, and dotted lines correspond to measurements after the first period of shear at $10\,\text{s}^{-1}$, after shear at $1\,\text{s}^{-1}$, and after the second period of shear at $10\,\text{s}^{-1}$, respectively.

the key parameter to control the defect density. Both ^{2}H NMR and rheology data suggested a reversible increase of the defect density as the shear rate was increased (within the lamellar region). Here, we investigate if these previously observed pretransitional defects are large enough to have an influence on the diffusion behavior. In one of the experiments described in the previous section, after the MLV-to-lamellae transition being completed at a shear rate of $10\,\text{s}^{-1}$, the shear rate was decreased to $0.1\,\text{s}^{-1}$ and, afterwards, increased back to $10\,\text{s}^{-1}$. Diffusion was measured after each shearing period, that is, at 10, 0.1, and $10\,\text{s}^{-1}$. Diffusion maps for the velocity and vorticity directions are shown on the left and right of Fig. 10, respectively. The diffusion profile for the velocity direction shows no perceptible changes. In the vorticity direction, however, diffusion becomes faster, when the shear rate is decreased. This change is reversible. Comparison of the D_w values for the different spatial directions shows that they are equal at the low shear rate. This is in good agreement with the model of nearly perfectly planar lamellae. The slower diffusion along the vorticity axis at the higher shear rate, on the other hand, points to structural defects which have a preferred orientation. A structure consistent
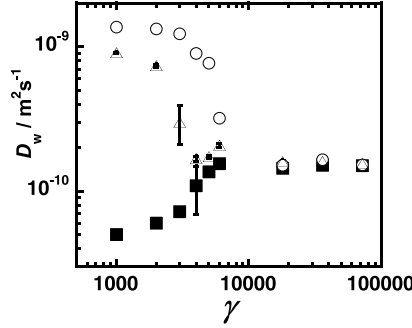
Fig. 11. Diffusion coefficients of water along the velocity (circles), vorticity (triangles), and velocity gradient (squares) directions during the transition from planar lamellae to MLVs at 34 °C and $\dot{\gamma} = 10\,\text{s}^{-1}$.

with the observed diffusion anisotropy are undulations with a wave vector in the vorticity direction. Such undulated structures have been suggested to occur also during the transformation form planar lamellae to MLVs at higher shear rates in the MLV regime of the shear diagram [16]. Thus, the pretransitional behavior observed in the regime of planar layers shows steady-state structures which are very similar to the transient intermediate structures postulated for the early stage of the lamellae-to-onion transition at higher shear rates.

3.3 Homogeneous transition from planar layers to multilamellar vesicles

We now turn to the complete transformation from planar layers to vesicles in the MLV region of the shear diagram as indicated by the arrow pointing downwards in the left panel of Fig. 1. The initial state was prepared by shearing at 43 °C and a shear rate of $10\,\text{s}^{-1}$ for 60 min. Then shear was stopped, the temperature was changed to 34 °C, and after thermal equilibration shear was started again at $10\,\text{s}^{-1}$. The diffusometry results are summarized in Figs. 11 and 12.

Figure 11 shows the strain dependence of the coefficients for water diffusion in the velocity, velocity gradient, and vorticity directions (D_{vel}, D_{grad}, and D_{vort} represented by circles, squares, and triangles, respectively). Besides a global increase of the diffusion constants, which is expected because of the higher temperature, Fig. 11 shows the same features of the strain-dependence of the diffusion anisotropy as reported previously for a temperature of 25 °C [16]. Thus, these new data are consistent with the previously described model of structural transformation: The initially planar lamellae ($D_{\text{vel}} = D_{\text{vort}} > D_{\text{grad}}$) at first become undulated, with the wave vector along the vorticity axis ($D_{\text{vel}} > D_{\text{vort}} > D_{\text{grad}}$). Subsequently, undulations with wave vectors along the velocity directions are added. The fission and fusion of the bilayer membranes occurs in an anisotropic way such that cylinder-like structures ($D_{\text{vel}} > D_{\text{vort}} = D_{\text{grad}}$) are formed, which finally transform into the isotropic MLV structure ($D_{\text{vel}} = D_{\text{vort}} = D_{\text{grad}}$). Even the strain scale, on which these processes occur, is the same for both temperatures. Figure 12 illustrates the change of the diffusion profiles across the gap during the transformation process (for the diffusion in the velocity direction, which undergoes the largest change). Throughout the transformation, D_{w} remains independent of
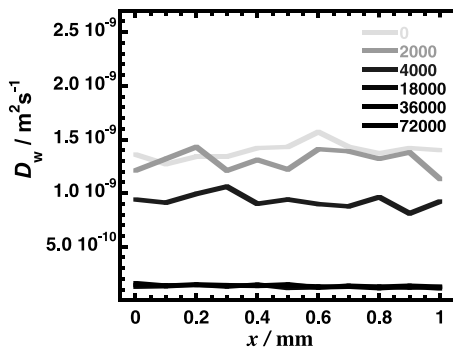
Fig. 12. Diffusion coefficient of water along the velocity direction as a function of the position in the gap for different strain values during the transition from planar lamellae to MLVs at 34 °C and $\dot{\gamma} = 10\,\mathrm{s}^{-1}$.
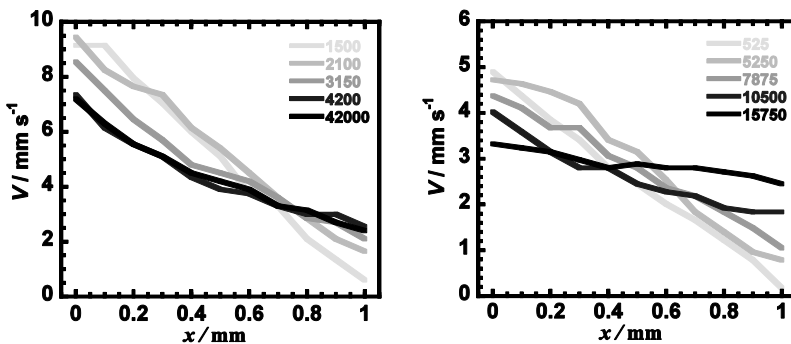

Fig. 13. Velocity profiles during the transition from planar lamellae to MLVs at 34 °C and shear rates of $10\,\mathrm{s}^{-1}$ (left) and $5\,\mathrm{s}^{-1}$ (right).

the position, confirming that the transformation from planar layers to vesicles is a homogeneous process.

In Fig. 13 velocity profiles are presented for the transition from planar layers to vesicles. The profiles on the left were obtained at the same shear rate $\dot{\gamma} = 10\,\mathrm{s}^{-1}$ as the diffusion data, while the profiles on the right were obtained in another experiment, carried out at $\dot{\gamma} = 5\,\mathrm{s}^{-1}$. As the transformation evolves, a gradual decrease in the slope of the velocity profile (corresponding to a decrease of the actual shear rate) combined with increasing wall slip is observed. With increasing strain, a curvature in the velocity profiles is noticed, in particular, at the higher shear rate, but there is no indication of discrete shear bands.

3.4 Structures in the transition region

The so called transition region depicted in the shear diagram of Fig. 1 is based on measurements of the steady-state viscosities as a function of shear rate [30]. It represents the region of shear rates, where shear thickening is observed, opposed to the shear thinning

of lamellae becoming aligned and onions becoming smaller in size [26]. Rheo-SANS experiments indicate that planar lamellae and onions may coexist here [33]. In most later investigations this region, which seems to separate the regimes of planar lamellae and MLVs, was deliberately avoided [16,27,29,43]. In the following we turn our attention towards this transition region. The structures at two points in this region, labeled T1 and T2 (shown in the right part of Fig. 1) are investigated. Diffusion coefficients, ^{2}H NMR spectra of heavy water, and velocities are analyzed. In total, four different types of jump experiments have been performed, such that each of the points T1 and T2 is approached starting from the stability regime of either planar lamellae (at higher temperature) or MLVs (at lower temperature). Thus we can clarify whether the steady-state structures in the transition region depend on the initial conditions.

All experiments were performed at a shear rate of $10\,\mathrm{s}^{-1}$. The initial states of MLVs and planar lamellae were prepared at 34 and 43 °C, respectively, by shearing for one hour. The temperatures of the target points are 40 °C for T1, which is close to the regime of stable layers, and 39 °C for T2 in the middle of the transition region. As in the experiments discussed before, the samples were sheared at the initial temperature, then shear was stopped during the temperature "jump" and the samples were allowed to thermally equilibrate for at least 40 min before, finally, shear was started again and the structural transformation at the target temperature was followed as a function of strain.

None of the four experiments revealed a discontinuity in the diffusion profiles across the gap indicating that the transformation process is homogeneous in all cases. Thus, if there is a coexistence of planar layers and vesicles, both structures are homogeneously distributed in the Couette gap. This is clearly different from the case described in Sect. 3.1 above, in which the jump is made from a state of MLVs into the stability region of planar lamellae, *cf.* Fig. 4.

Figure 14 shows how the anisotropy of the diffusion coefficients (averaged over the gap) evolves as a function of strain. The upper and lower rows of plots display the data for the target points T1 and T2, respectively, while the left and right columns represent the different initial conditions, that is, MLVs and aligned layers, respectively. Note that for the right column strain increases from right to left so that the diffusivities at the respective target points are shown "face to face" in the middle of each row.

When starting from MLVs and jumping to T1 (upper left of Fig. 14, diffusion initially is nearly isotropic as expected for MLVs but it becomes anisotropic, with a small increase of D_w in both velocity and vorticity directions and a simultaneous decrease in the gradient direction. Hence, the data seem to indicate a progressive formation of a lamellar-like structure. However, the process is much slower and the final diffusion anisotropy is smaller compared with a jump across the transition region. When T1 is approached from an initial state of aligned lamellae (upper right of Fig. 14) the initial anisotropy is reduced somewhat. A slight decrease in D_w in the velocity and vorticity directions is accompanied by an increase in D_w in the velocity gradient direction. Also, the difference between the diffusivities in the velocity and vorticity directions becomes larger. The structural changes when approaching T1 from aligned layers appear to be much less pronounced compared to the MLV-to-T1 transition. However, for all three spatial directions, the final diffusion coefficients are the same, independent of the initial structure of the system.
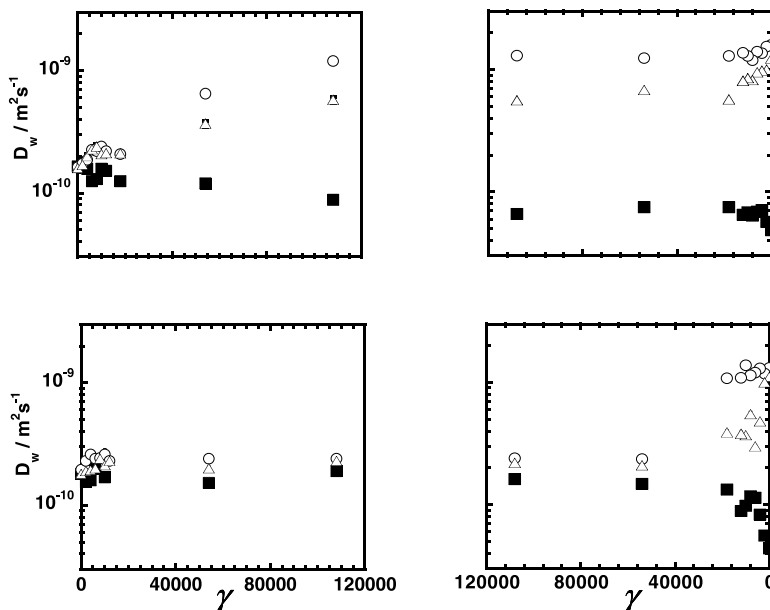
Fig. 14. Diffusion coefficients of water during the transitions to points T1 (top) and T2 (bottom) in the transition region of the shear diagram, starting from different initial states. Left: the initial state consists of MLVs generated at 34 °C, right: initial state of planar lamellae generated at 43 °C. The strain axis has been reversed in the right column for better comparison of corresponding final states at high strain. The circles, triangles, and squares represent diffusion coefficients in the velocity, vorticity, and velocity gradient direction, respectively.

This is also the case for T2 as target point. After shearing, an almost isotropic structure is obtained. When the target state is approached starting from MLVs there is hardly any change in the D_w values, except for a slight overall increase in the beginning of the transformation at strains below 1000. When starting from layers and jumping to T2 the initial anisotropy vanishes almost completely. Altogether, the diffusivities suggest that the structure of T1 is closer to layers, while T2 resembles MLVs. This indicates a gradual change of the steady-state structures as temperature is changed within the transition region.

In Fig. 15, the ^{2}H NMR spectra of heavy water in the initial and final states of the jump experiments are compared. The left and right parts of Fig. 15 show the experiments with T1 and T2, respectively, as final state. In each case, solid and dotted lines (with higher maximum) correspond to transformations starting from aligned layers and MLVs, respectively. Thus, they represent the initial states – a broad single peak for MLVs and a doublet for planar lamellae. The two superimposed spectra of lower height in each set were obtained when the samples had reached their final states. The small shoulder in the left peak arises most likely from a poorly mixed sample which leads to the superposition of slightly different spectra. This is often observed and does not affect onion formation.
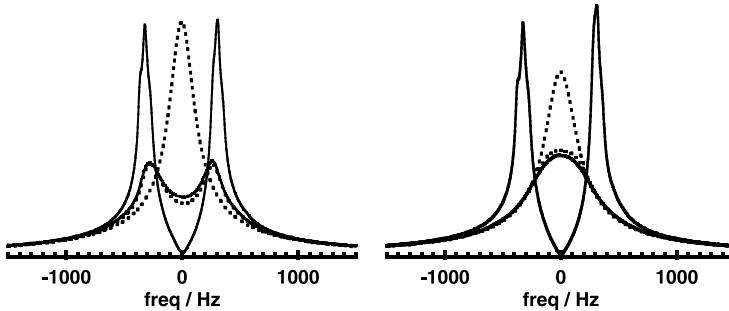
Fig. 15. Initial and final ^{2}H NMR spectra for the transformations observed at points T1 (left) and T2 (right) in the transition region. In each case, solid lines represent the transformation starting from aligned lamellae (doublet with large splitting) and dotted lines correspond to the transformations starting from MLVs (single peak with higher maximum intensity). The spectra of the final states have an intermediate shape that is different for T1 and T2 but independent of the initial structure.

The almost perfect agreement of the superimposed spectra makes evident that the final state does not depend on the history of the samples. For both T1 and T2 as target points, the final structure is distinctly different from both initial structures. While the spectra of T1 still show a splitting, the spectra of T2 consist of a single but very broad peak. In other words, the steady-state structure at the higher temperature (T1) is more similar to planar lamellae than to MLVs, whereas the one at the lower temperature (T2) resembles MLVs, in good agreement with the diffusometry results.

Although the spectra of the final states T1 and T2 can be fitted by superpositions of three Lorentzian lines (corresponding to one doublet and a broad central peak) they are clearly not a sum of the spectra observed in the two regions above and below the transition region. The spectral splitting of the doublet in state T1 is much smaller than the splitting in the regime of aligned lamellae and suggests a less ordered state. Likewise, the spectra in state T2 are much broader than the MLV spectra at lower temperatures, indicating that the bilayers comprising the structure are less curved than in the MLV region. There is also no evidence of shoulders which would indicate an underlying doublet resulting from planar lamellae. Therefore, we can rule out the coexistence of large domains of aligned layers and MLVs in the transition region. The NMR spectra point towards a homogeneous structure, intermediate between perfect layers and MLVs and changing continuously as one passes through the transition region. A superposition of two structures appears less likely, although inhomogeneities on a length scale smaller than a few μm, as estimated from the mean square displacement of water due to self diffusion during the time scale of the NMR measurement, cannot be excluded.

The velocity profiles, depicted in Fig. 16 for the four experiments involving the transition region, further support the model of well-defined steady-state structures in the transition region. There is no evidence of shear banding. In the initial stage of the transformation "MLV to T1" (Fig. 16, upper left), there is considerable wall slip, and the shear rate decreases somewhat as the strain is increased. At a later stage, the shear rate increases approximately to its applied value and the wall slip disappears. The first
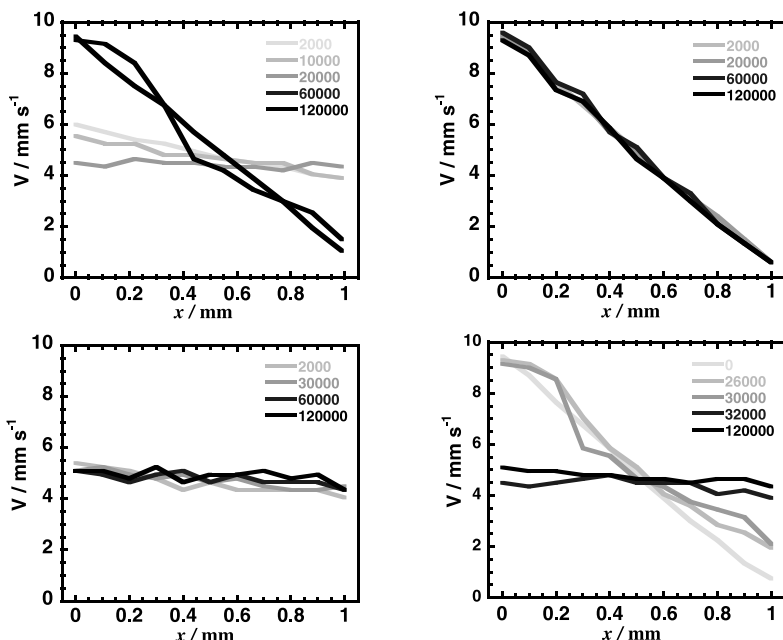
Fig. 16. Velocity profiles during the transitions to points T1 (top) and T2 (bottom) in the transition region of the shear diagram, starting from different initial states. Left: the initial state consists of MLVs generated at 34 °C, right: initial state of planar lamellae generated at 43 °C.

part of the process may indicate a growth of MLVs, *e.g.*, by fusion of smaller vesicles. Larger MLVs are known to exhibit a higher viscosity, hence the observed decrease of the shear rate. Eventually, some of the MLVs may be disrupted and a matrix of aligned planar lamellae may form. Due to the low viscosity of aligned lamellae the shear rate increases.

For the transition from planar lamellae to T1 (Fig. 16, upper right), no changes in the velocity profile are observed and the curves for all strains fall on one line. This is in agreement with the relatively small changes observed by diffusometry and spectroscopy: the initial and final states are structurally related; also the final state is layer-like.

The velocity profiles obtained during the MLV-to-T2 transformation (Fig. 16, lower left) confirm that there are no major changes during this transition. There is a very small decrease of the average shear rate, which is much smaller than the applied shear rate because of considerable wall slip. The decrease in shear-rate indicates an increase in viscosity, which can be explained by the increase in MLV size as indicated by spectral line shapes.

Finally, the transformation from planar layers to T2 (Fig. 16, lower right) shows a change from a high shear rate to lower shear rates with significant wall slip, just in reverse to the changes observed during the MLV-to-T1 transformation. This is in agreement with T2 being more closely related to MLVs than to planar layers, in agreement with the results from diffusometry and spectroscopy.

3.5 Wall slip

In many of the velocity profiles discussed here, wall slip is evident. In the absence of slip, the velocity at the stationary outer wall is zero and, for shear rates of 10, 5, and $2.5\,\mathrm{s}^{-1}$ and a gap of 1 mm thickness, it is 10, 5, and $2.5\,\mathrm{mm\,s}^{-1}$, respectively, at the inner moving wall. This is approximately given when the shear bands disappear during the MLV-to-layer transformation, seen in Figs. 5 and 8, and in all cases when the structure consists of planar lamellae, for instance, in the initial stages of the layer-to-MLV transformation (Fig. 13). On the other hand, MLVs always show strong wall slip, which is evident, for example, in Figs. 13 and 16. Although the velocity profiles may become fairly flat in the onion state, a small shear rate is always maintained within the sample. If plug flow occurred the measured tangential velocity would slightly increase with the radius; this phenomenon is not observed. From an inspection of all velocity profiles we may conclude that wall slip is a characteristic feature of the MLV structure and does not occur in samples consisting of aligned layers.

We may now return to Fig. 4 and the increased diffusivity at the outer wall that is observed during the shear-banded transformation from MLVs to planar lamellae. If the velocity at the stationary outer wall is larger than zero and a contact between wall and sample remains there must be a third shear band with a very high shear rate close to the outer wall. This band obviously consists of aligned layers having high diffusivities. In some cases it is so narrow that it is missed in the experiments which have a limited resolution. Applying the so called lever rule, by which the total shear rate is calculated as a weighted sum over the observed bands, to the shear banding profiles during the MLV-to-layer transition, *cf.* Fig. 5, we obtain total shear rates smaller than the applied values. This provides further evidence of a missing narrow high-shear band at the outer wall.

In the MLV state slip occurs at both walls, reducing the measured velocity in the voxel at the inner wall and increasing it at the outer wall. Obviously, the major part of the total shear occurs close to the walls in layers too thin to be seen in our NMR velocimetry experiments, while the bulk of the sample undergoes very little shear.

4. Conclusions

The rheo-NMR experiments reported here have shown that the transformation from MLVs to aligned planar lamellae after a jump in temperature across the socalled transition region of the shear diagram is accompanied by a transient gradient shear banding. Two bands can be observed: a band of high shear rate consisting of aligned lamellae next to the moving wall of the shear cell and a band of low shear rate consisting of the initial MLV structure close to the outer stationary wall. This shear banding scales with the applied strain. Upon increasing strain, the boundary between the two bands is shifted towards the outer wall until the MLV band disappears. High diffusivity and wall slip at the outer wall as well as failure of the lever rule indicate the existence of an additional narrow band of high shear rate consisting of aligned layers at the outer wall. Wall slip is found to be a characteristic and reproducible feature of the onion state.

No discrete shear bands are resolved by NMR velocimetry when MLVs are formed during the homogeneous transformation starting from an initial state of well aligned layers. However, a formation of regions of high shear rate at both walls must be pos-

tulated to account for the observed wall slip and the low actual shear rate evident from the velocity profiles in the MLV state.

The shear-induced structures are independent of the history of the samples. This holds true also in the transition region. Here, steady states are found, the structures of which change continuously from being layer-like at higher temperatures to onion-like at lower temperatures. NMR spectroscopy suggests that the structures in the transition region are homogeneous on a length scale above a few micrometers.

Acknowledgement

References

1. P. T. Callaghan, Rep. Prog. Phys. **62** (1999) 599.
2. C. Schmidt, TS , in: *Modern Magnetic Resonance*, G. A. Webb (Ed.) Springer, New York (2008), pp. 1515–1521.
3. P. T. Callaghan, Curr. Opin. Colloid. In. **11** (2006) 13.
4. N. Dingenouts and M. Wilhelm, Korea-Australia Rheol. J. **22** (2010) 317.
5. H. S. Melito and C. R. Daubert, Ann. Rev. Food Sci. Technol. **2** (2011) 153.
6. A. I. Nakatani, M. D. Poliks, and E. T. Samulski, Macromolecules **23** (1990) 2686.
7. D. A. Grabowski and C. Schmidt, Macromolecules **27** (1994) 2632.
8. Y. Xia and P. T. Callaghan, Macromolecules **24** (1991) 4777.
9. P. T. Callaghan, *Principles of Nuclear Magnetic Resonance Microscopy*, Clarendon Press, Oxford (1993).
10. A. Lutti and P. T. Callaghan, Phys. Rev. E **73** (2006) 011710.
11. A. Lutti and P. T. Callaghan, J. Magn. Reson. **180** (2006) 83.
12. A. Lutti and P. T. Callaghan, J. Magn. Reson. **187** (2007) 251.
13. A. Lutti and P. T. Callaghan, Eur. Phys. J. E **24** (2007) 129.
14. A. Lutti and P. T. Callaghan, Appl. Magn. Reson. **33** (2008) 293.
15. I. Åslund, B. Medronho, D. Topgaard, O. Söderman, and C. Schmidt, J. Magn. Reson. **209** (2011) 291.
16. B. Medronho, J. Brown, M. G. Miguel, C. Schmidt, U. Olsson, and P. Galvosas, Soft Matter **7** (2011) 4938.
17. H. W. Spiess, Adv. Polym. Sci. **66** (1985) 23.
18. E. O. Stejskal and J. E. Tanner, J. Chem. Phys. **42** (1965) 288.
19. J. E. Tanner, J. Chem. Phys. **52** (1970) 2523.
20. R. G. Larson, *The Structure and Rheology of Complex Fluids*, Oxford University Press, New York, Oxford (1999).
21. C. R. Safinya, E. B. Sirota, R. F. Bruinsma, C. Jeppesen, R. J. Plano, and L. J. Wenzel, Science **261** (1993) 588.
22. O. Diat and D. Roux, J. Phys. II **3** (1993) 9.
23. O. Diat, D. Roux, and F. Nallet, J. Phys. II **3** (1993) 1427.
24. O. Diat, D. Roux, and F. Nallet, J. Phys. IV **3(C8)** (1993) 193.
25. D. Roux, F. Nallet, and O. Diat, Europhys. Lett. **24** (1993) 53.
26. S. Müller, C. Börschig, W. Gronski, C. Schmidt, and D. Roux, Langmuir **15** (1999) 7558.
27. B. Medronho, S. Shafaei, R. Szopko, M. G. Miguel, U. Olsson, and C. Schmidt, Langmuir **24** (2008) 6480.
28. M. Lukaschek, S. Müller, A. Hasenhindl, D. A. Grabowski, and C. Schmidt, Colloid Polym. Sci. **274** (1996) 1.

TS Please add the title of the chapter.

Editor's or typesetter's annotations (will be removed before the final TeX run)

29. B. Medronho, C. Schmidt, U. Olsson, and M. G. Miguel, Langmuir **26** (2010) 1477.

30. C. Oliviero, L. Coppola, R. Gianferri, I. Nicotera, and U. Olsson, Colloid. Surface. A **228** (2003) 85.

31. T. D. Le, U. Olsson, K. Mortensen, J. Zipfel, and W. Richtering, Langmuir **17** (2001) 999.

32. J. Zipfel, F. Nettesheim, P. Lindner, T. D. Le, U. Olsson, and W. Richtering, Europhys. Lett. **53** (2001) 335.

33. F. Nettesheim, J. Zipfel, U. Olsson, F. Renth, P. Lindner, and W. Richtering, Langmuir **19** (2003) 3603.

34. F. Nettesheim, U. Olsson, P. Lindner, W. Richtering, J. Phys. Chem. B **108** (2004) 6328.

35. B. Medronho, S. Fujii, W. Richtering, M. G. Miguel, U. Olsson, Colloid Polym. Sci. **28** (2005) 317.

36. S. Fujii and W. Richtering, Eur. Phys. J. E **19** (2006) 139.

37. B. Medronho, M. G. Miguel, and U. Olsson, Langmuir **23** (2007) 5270.

38. S. Koschorek, S. Fujii, and W. Richtering, Prog. Theor. Phys. Suppl. **175** (2008) 154.

39. S. Koschoreck, S. Fujii, P. Lindner, and W. Richtering, Rheol. Acta **48** (2009) 231.

40. S. Fujii, S. Koschorek, P. Lindner, and W. Richtering, Langmuir **25** (2009) 5476.

41. S. Fujii, Prog. Colloid Polym. Sci. **136** (2009) 69.

42. L. Filippelli, B. Medronho, C. O. Rossi, M. G. Miguel, and U. Olsson, Mol. Cryst. Liq. Cryst. **500** (2009) 166.

43. M. Medronho, B. Rodrigues, M. G. Miguel, U. Olsson, and C. Schmidt, Langmuir **26** (2010) 11304.

44. R. Weigel, J. Läuger, W. Richtering, and P. Lindner, J. Phys. II **6** (1996) 529.

45. T. D. Le, U. Olsson, and K. Mortensen, Phys. Chem. Chem. Phys. **3** (2001) 1310.

46. T. Kato, K. Miyazaki, Y. Kawabata, S. Komura, M. Fujii, and M. Imai, J. Phys.: Condens. Matter **17** (2005) S2923.

47. K. Miyazaki, Y. Kosaka, Y. Kawabata, S. Komura, and T. Kato, J. Appl. Crystallogr. **40** (2007) s332.

48. Y. Suganuma, M. Imai, T. Kato, U. Olsson, and T. Takahashi, Langmuir **26** (2010) 7988.

49. Y. Kosaka, M. Ito, Y. Kawabata, and T. Kato, Langmuir **26** (2010) 3835.

50. L. Gentile, C. O. Rossi, U. Olsson, and G. A. Ranieri, Langmuir **27** (2011) 2088.

51. L. Gentile, K. Mortensen, C. O. Rossi, U. Olsson, and G. A. Ranieri, J. Colloid Interface Sci. **362** (2011) 1.

52. M. Ito, Y. Kosaka, Y. Kawabata, and T. Kato, Langmuir **27** (2011) 7400.

53. J. Zhou, J. Yang, X. Chen, W. Luo, W. Zhang, K. Yang, and B. Zhang, J. Mol. Struct. **987** (2011) 91.

54. L. Gentile, C. O. Rossi, and U. Olsson, J. Colloid Interface Sci. **367** (2012) 537.

55. L. Gentile, B. F. B. Silva, S. Balog, K. Mortensen, and U. Olsson, J. Coll. Interface Sci. **372** (2012) 32.

56. G. Auernhammer and H. R. Brand, Phys. Rev. E **66** (2002) 061707.

57. P. D. Olmsted, Rheol. Acta **47** (2008) 283.

58. S. M. Fielding, Soft Matter **3** (2007) 1262.

59. S. Manneville, Rheol. Acta **47** (2008) 301.

60. P. T. Callaghan, Rheol. Acta **47** (2008) 243.

61. G. M. H. Wilkins and P. D. Olmsted, Eur. Phys. J. E **21** (2006) 133.

62. H. A. Barnes, J. F. Hutton, and K. Walters, *An Introduction to Rheology*, Elsevier, Amsterdam (1989).

63. S. A. Rogers and P. T. Callaghan, Rheol. Acta **48** (2009) 735.

64. P. T. Callaghan, C. D. Eccles, and Y. Xia, J. Phys. E **21** (1988) 820.

65. M. Lukaschek, D. A. Grabowski, and C. Schmidt, Langmuir **11** (1995) 3590.

66. S. Müller, P. Fischer, and C. Schmidt, J. Phys. II **7** (1997) 421.